

# REMOTE SENSING OF THE OCEAN-SURFACE WIND FIELD WITH A SCATTEROMETER AND A SYNTHETIC APERTURE RADAR

By detecting kilometer-scale variations in the wind field at the ocean surface, the Seasat synthetic aperture radar can provide information on both wind speed and direction. Although the environmental limits of this technique are not yet known, such an application would allow research on scales of surface wind field variability that are presently not available.

## INTRODUCTION

Knowledge of the ocean-surface wind field is useful to a wide range of activities, both theoretical and applied. Ocean-circulation models and surface-wave models require the ocean-surface wind field as an input (see the article by McGoldrick in this issue). Moreover, the winds play a role in generating internal waves and in mixing in the upper ocean. A knowledge of ocean-surface winds also has practical importance in short-range weather forecasting, ship routing, resource exploration, and commercial fishing.

Conventional estimates of ocean winds vary substantially in their coverage, resolution, and nature. Global estimates are obtained primarily by satellite cloud imagery, and through ship reports of surface wind speed and direction, and surface pressure. In coastal regions, buoys and island weather stations provide additional information. In the tropics, the presence of large-scale winds can be inferred by tracking cloud motions in images from geostationary satellites. These measurement techniques are sufficiently diverse that even when they are nearly coincident temporally and spatially, differences are often considerable. For example, winds obtained from tracks of cloud motion may differ very substantially from winds at surface level. Ship observations are generally confined to well-traveled routes located primarily in the northern hemisphere. In the southern hemisphere, observations are sparse, and information must be obtained primarily from satellite imagery. Thus, in global ocean wind observations, there is a large deficiency that potentially could be filled through microwave remote sensing by satellites.

Seasat was the first research satellite dedicated to microwave remote sensing over the ocean. It carried an altimeter, wind field scatterometer (SASS), scanning multichannel radiometer, synthetic aperture radar (SAR), and a visible and infrared radiometer. The Seasat instruments are described in detail in Ref. 1, and many of the scientific results obtained using Seasat data are contained in Refs. 2, 3, and 4.

For synoptic-scale atmospheric forecast models, as well as for most ocean circulation models, the nominally 50-kilometer resolution of SASS is probably adequate and is, in fact, much better than that obtainable through conventional measurements. However, near land, fronts, squall lines, and rain cells, and in environments of high wind gradient, observations of a higher resolution than that possible with SASS would be desirable. Also, as McGoldrick points out, mesoscale eddy circulation may be driven to some extent by the fine-scale wind structure. The high spatial resolution of SAR makes it a potential candidate for observation of the wind field in all of these areas.

## DATA SET FROM PASS 1339

In the entire Seasat SAR data set, one pass has been particularly interesting because of the comprehensive set of simultaneous and coincident measurements that were made. Seasat pass 1339, containing a 900-kilometer segment of the ocean located just east of Cape Hatteras, N. C., occurred on September 28, 1978, at approximately 1520 Greenwich Mean Time. A National Oceanic and Atmospheric Administration P-3 aircraft flew at 150 meters altitude along a path roughly coincident with the northern 600 kilometers of the SAR data set and made estimates of wind speed and direction based on its inertial navigation system, as well as of air and sea temperatures. Figure 1 shows the geometry of pass 1339, including the location of SASS and the aircraft measurements of wind direction. A pressure trough, indicated on the National Weather Service surface chart, cuts through the southern end of the region of interest.

A SASS wind field solution may specify two, three, or four ambiguous estimates<sup>5</sup> of wind speed and direction. Variations among the wind speed estimates are typically small, but the direction estimates may differ substantially. If there are just two solutions, they will be separated by 180 degrees, while four solutions may be nearly orthogonal. In other studies, the SASS estimates of wind speed have been found to be accurate

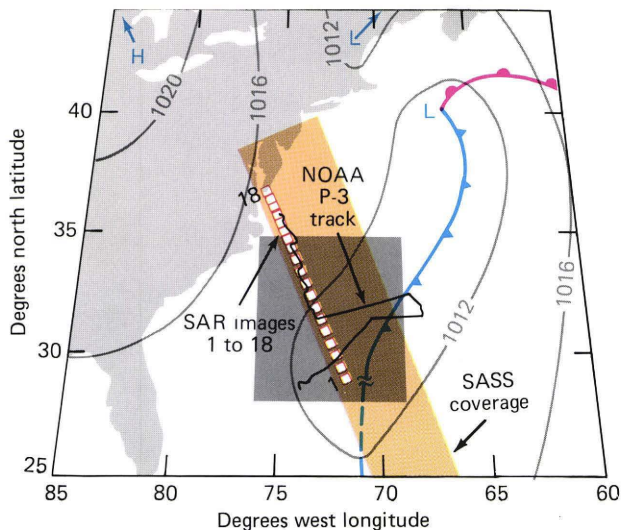


**Figure 1**—Region of Seasat pass 1339 with information taken from the National Weather Service surface chart of 1200 Greenwich Mean Time on the day of Seasat overpass. Also indicated is the area covered by SASS, locations of 40-kilometer-square SAR images, and the National Oceanic and Atmospheric Administration's P-3 aircraft subtrack. The enclosed rectangular area marks the region shown in Fig. 10.

to within  $\pm 2$  meters per second and the wind direction (once selected from the various possibilities) to within  $\pm 20$  degrees.<sup>5</sup> Thus, even with the problems associated with making the SASS wind field solutions unambiguous, this instrument is generally considered a success, and an improved scatterometer will be flown on the Navy Remote Ocean Sensing System scheduled for launch in 1989.

The weak front shown in Fig. 1 is not well determined by the existing pressure data; an examination of the National Weather Service surface pressure charts shows that only a few ship observations were located in the vicinity and that some of these were spurious. However, the existence of the front is confirmed by the observations of the wind field in the experiment, although even with this information, the location remains uncertain to within perhaps 75 kilometers.

The SAR images were produced by MacDonald, Dettwiler and Associates (MDA) of Vancouver, Canada, in the form of 40-kilometer-square, digitally processed plots at a 25-meter resolution (four looks). The locations of the images are shown in Fig. 1. From this data set, 114 nearly contiguous images of 6.4-kilometer-square regions were extracted. Beal et al.<sup>6</sup> discuss the imagery and its analysis for wave studies. Here, however, only the wind speed estimates derived from this data set are discussed.

To provide a better description of the SAR spectral signature of the wind field and to obtain an estimate more nearly commensurate with the nominal 50-kilometer resolution of SASS, eighteen 25.6-kilometer-square images were also extracted from the original MDA imagery. The images were derived from the original imagery by subsetting a 1024 by 1024 pixel (12.5-meter pixel size) section and then averaging square

groups of 8 by 8 pixels, yielding a 256 by 256 pixel image with 100-meter pixels. The lowest frequency resolved in the spectra of this imagery corresponds to 25.6 kilometers, and the Nyquist limit corresponds to 200 meters.

Finally, to assess the SAR's ability to provide high-resolution directional measurements of the wind field, a 38.4-kilometer-square subimage was extracted from each of the original MDA images and partitioned into a 6 by 6 array of 6.4-kilometer-square images. Estimates extracted from this set of images provide a two-dimensional view of the wind field that is more revealing than the basically linear arrangement of 25.6-kilometer-square SAR images.

For each of the image sets, discrete Fourier transforms were computed and direction estimates were derived. Spectral analysis is a natural methodology to use for this problem since the wind and wave signatures occur on distinct scales and, in the most explicit cases, the wind-direction signature corresponds to a spectral peak. Moreover, variability estimates can be derived for the parameters of interest using standard least-squares theory.

Figure 2 is a composite of the eighteen 25.6-kilometer-square MDA SAR images whose locations are shown in Fig. 1. Much information is contained in this set of images. Average brightness is generally related to the wind speed, although dark regions, such as in image 6, may also be the result of the 30-centimeter Bragg waves being damped by rain. Wave modulation occurs on a scale too small to be evident in these images, although it is very clearly revealed in spectra. Linear features, probably caused by current gradients (see the article by Thompson in this issue), occur in images 13 to 18. Linear streaks, believed to be the surface expression of atmospheric roll vortices, are also evident in some of the images, such as images 4 and 10.

## SASS AND SAR ESTIMATES OF WIND SPEED

Since ocean-surface roughness is related to wind speed and since average backscatter intensity for SAR is related to ocean-surface roughness, it is possible in principle to derive wind speed over the ocean from the SAR measurements. In practice, the Seasat SAR had several limitations that precluded obtaining absolute estimates of wind speed. Because the Seasat SAR was not absolutely calibrated, the absolute radar cross section of the ocean cannot be derived from the intensity of the returned signal. Also there is substantial and only partially correctable range variability because of the antenna beam pattern, as well as larger scale variations because of changes in spacecraft attitude. In spite of these limitations, it is possible to use the Seasat data to estimate relative wind speed. Samples taken at a constant range within a single satellite pass should possess good relative radiometric stability, and measured variations in mean backscatter intensity should be related to real variations in the surface wind magnitude.

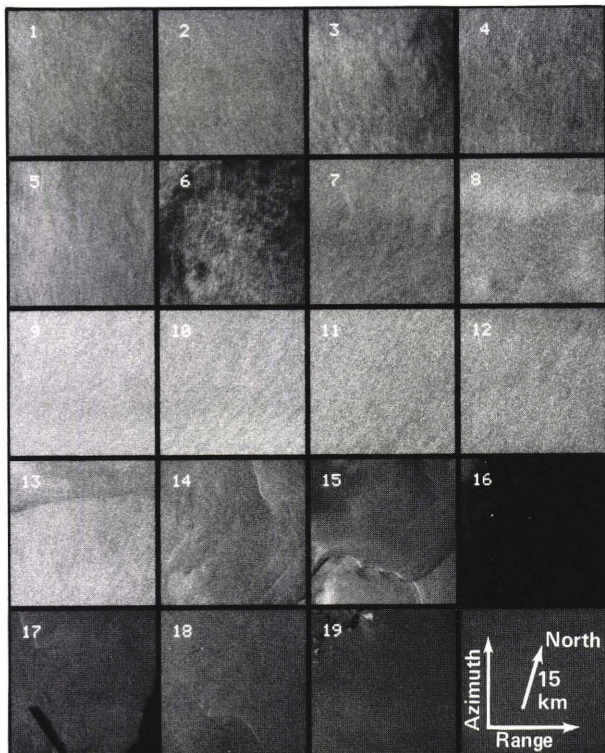


Figure 2—Eighteen 25.6-kilometer-square SAR images. The numbering is consistent with Fig. 1.

The data set from pass 1339 provides an excellent means to test this hypothesis. We have assumed a simple power-law relationship, with two adjustable parameters, relating wind speed as measured by SASS to mean backscatter intensity from SAR. Specifically, we assume

$$\sigma_0 = KU^a, \quad (1)$$

where  $U$  is SASS-estimated wind speed at 19.5 meters above the sea surface,  $\sigma_0$  is SAR-measured backscatter averaged over 6.4-kilometer-square regions, and  $K$  and  $a$  are adjustable parameters. The resulting comparison of the two instruments is shown in Fig. 3.

Each SASS estimate of wind speed at a SAR image location was obtained through an interpolation of three SASS estimates that are closest to and that also triangulate the SAR image location. The three SASS estimates used are always within 40 kilometers of the corresponding SAR image location.

The SAR observations used to determine the fit are located between 29 and 35.5 degrees north. Four observations that were substantially lower than the others as a result of the high resolution of the SAR imagery were not included in the curve fit; neither were six observations derived from image 10 of Fig. 2 that appeared to be abnormally large. The first two of these six observations are located on a bright constant-azimuth band that may be an artifact of the SAR processor. The ten observations are plotted individually in Fig. 3. Agreement is excellent over the entire range

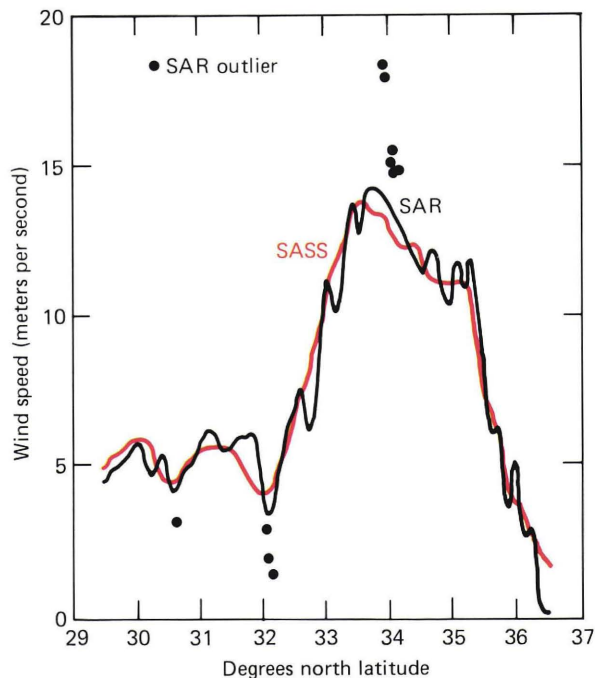


Figure 3—Wind speeds measured by SASS and SAR for pass 1339. SAR wind estimates were produced with  $\sigma_0 = KU^a$ , with  $a = 0.40 \pm 0.02$  and  $K = 464 \pm 12$ . The estimates were obtained through a best fit of SAR-measured backscatter to SASS-estimated winds (at 19.5 meters above the sea surface). Observations labeled "SAR outlier" were not included in the fit.

but with a small bias in the region between 29 and 32 degrees north. Values of  $a = 0.40 \pm 0.02$  and  $K = 464 \pm 12$  produced the least root-mean-square error in the fit, which is 0.7 meter per second.

### SASS AND SAR ESTIMATES OF WIND DIRECTION

In general, a relationship involving relative wind direction as well as wind speed is used to model radar backscatter from the ocean:<sup>7,8</sup>

$$\sigma_0 = KU^a [1 + b \cos(2\phi) + c \cos \phi], \quad (2)$$

where  $U$  and  $\sigma_0$  are defined as in Eq. 1 and  $\phi$  is relative wind direction (the azimuth look direction of the radar subtracted from the wind direction). Figure 4 plots the dependence of backscatter on relative wind direction for various wind speeds. The coefficient  $b$ , which is small and positive, accounts for decreased backscatter crosswind, while  $c$ , which is also positive but smaller than  $b$ , accounts for decreased backscatter when the radar look direction is downwind.

This analysis and others<sup>8</sup> have been inconclusive regarding the significance of the direction-dependent terms for L-band backscatter from Seasat SAR. However, the directional dependence of radar backscatter is the basis for the SASS estimate of wind direction. The SASS, which had four orthogonal antennas, made 15 radar backscatter measurements (at Ku band) per

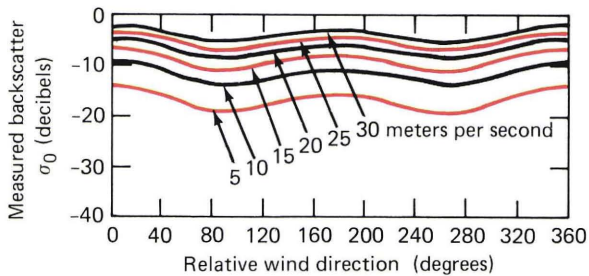


**Figure 4**—The dependence of  $\sigma_0$  on azimuth angle and wind speed (from the SASS geophysical model function using horizontal polarization, 30-degree incidence angle).

pulse with each antenna (see Fig. 5). Each measurement had a nominal footprint of approximately 60 by 20 kilometers, and the SASS wind algorithm used pairs of overlapping cells from the forward and aft antennas. Wind speed and direction estimates were derived from these measurements with a nominal resolution equivalent to a 50-kilometer square. However, with two orthogonal looks at each measurement location, there is still directional ambiguity. The SASS algorithm typically specified four possible solutions; the “correct” one is generally selected from supplementary information and larger scale patterns in the data.<sup>9</sup>

In this analysis, the SAR wind direction estimates are not determined from the anisotropy of radar backscatter with relative wind direction. In fact, such a determination would be impossible since the SAR observes each location essentially from only one relative wind direction. Rather, the estimates of wind direction are derived from the kilometer-scale variations in the L-band radar backscatter, which can reveal ocean surface expressions of atmospheric structures such as roll vortices, and are roughly aligned with the local wind direction. However, the cause of these features in SAR imagery is not fully understood and might simply be variations in surface wind speed or increased concentrations of surfactants. Other effects such as surface-current shear, internal waves, and rain also influence kilometer-scale SAR backscatter.<sup>10</sup> SAR will provide useful wind-direction information only if other effects can be separated from the wind effects or if they are typically not dominant.

To illustrate the surface wind expression in SAR imagery, Fig. 6 shows two enhanced 40-kilometer-square SAR images taken from widely separated portions of the pass. The top image (labeled 1 in Fig. 2) is from the low wind (3 to 5 meters per second) southern end of the pass, and the bottom image (labeled 10 in Fig. 2) is from the high wind (12 meters per second) mid-section of the pass. The pixel size is 50 meters, and the prominent linear structure that is evident is in a scale of kilometers. The structure is roughly aligned with the wind direction as determined from all available observations. The smaller scale variability may actually represent real variability in the wind field, although in the absence of surface measurements, this possibility must remain ambiguous. The structure in the lower image is better defined and consists of long

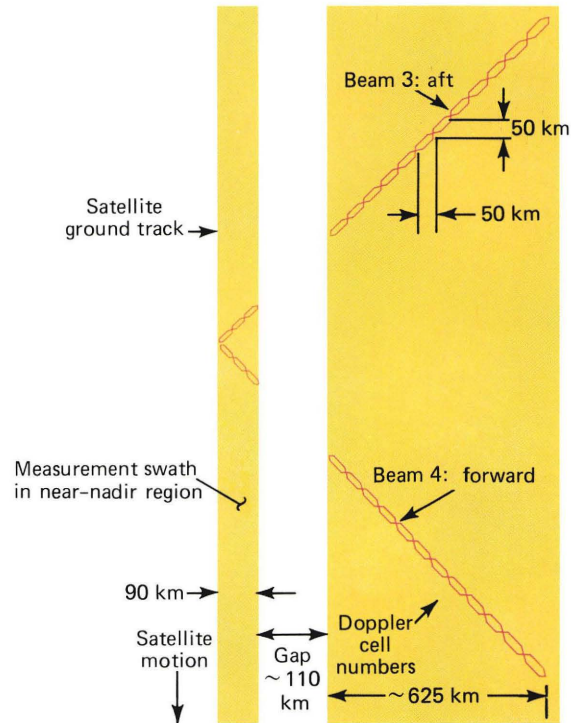


**Figure 5**—Cell geometry for Seasat SASS (derived from *Seasat Geophysical Data Record Users Handbook*).

bands that are oriented in the wind direction (toward the lower left of the image). This banded structure is probably the surface expression of well-developed atmospheric roll vortices.

Roll vortices, or windrows, are counterrotating helical circulations in the earth’s planetary boundary layer that are roughly aligned with the mean wind direction.<sup>11</sup> A schematic drawing of a typical roll vortex is shown in Fig. 7, adapted from Ref. 11. The horizontal spacing between regions of downward flow is typically about twice the height of the roll vortices, which in turn is related to the depth of the boundary layer. Windrows have been observed as cloud “streets” at the top of the boundary layer. They are also manifest in photographs of the sea surface, in the spacing of sand dunes, and even in the soaring pattern of seagulls. In the latter example,<sup>12</sup> seagulls were observed to soar in a linear pattern (hypothetically supported by the updraft between two rolls) in environments with air-sea temperature differences greater than 3°C and wind speeds of 7 to 13 meters per second. A typical horizontal spacing between roll vortices is 1 to 8 kilometers. Wavelengths as short as 0.3 kilometer have been observed through cloud streets in early morning, at a time when the convection layer is rapidly growing.

Roll energy can be supplied by either dynamical or convective instabilities in the planetary boundary layer. Theoretical models estimate roll orientation by determining the direction of maximum growth for these instabilities relative to the mean wind direction. The estimated direction and wavelength vary with the vertical velocity profile of the planetary boundary layer, the type of instability being modeled, and also with

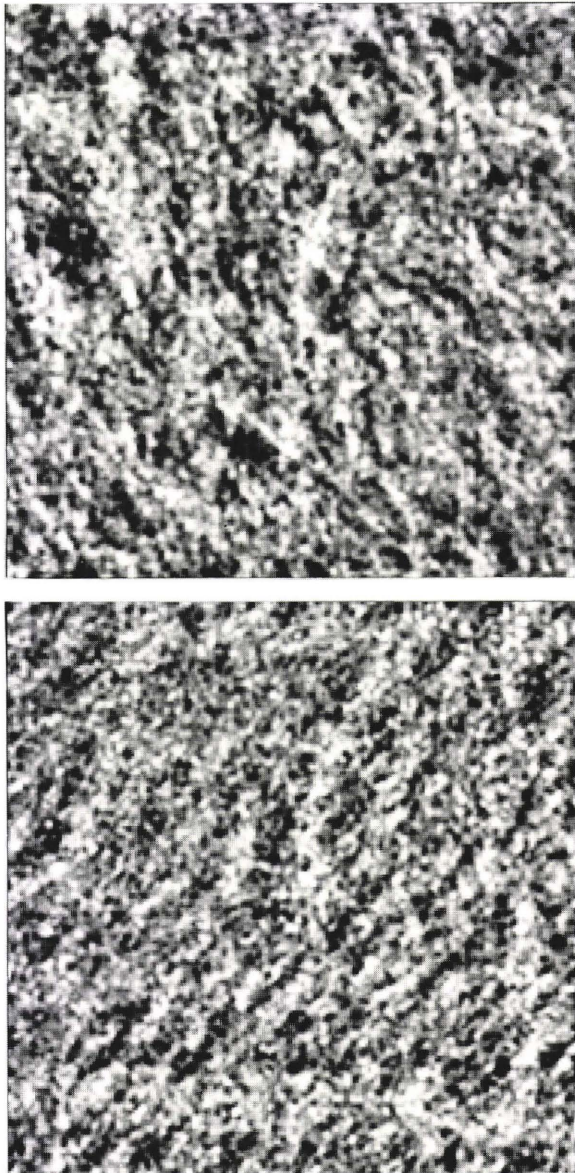


**Figure 6**—Enhanced 40-kilometer-square SAR images 1 (top) and 10 (bottom). The numbering is consistent with Fig. 2. The banded structure is aligned with the direction of local wind.

the complexity of the model. Positive buoyancy acts to align the rows with the mean velocity. Generally, the models yield no simple conclusion as to the directionality of the rolls. However, they do predict that the onset of the flows might occur at wind speeds of approximately 5 to 7 meters per second or at even lower speeds if the dominant instabilities are convective.

Figure 8 shows the set of 18 spectra of the 25.6-kilometer-square images shown in Fig. 2. The spectra were truncated so that the range of wavelengths displayed on each axis is 25.6 to 0.8 kilometers. The peak in the lower right quadrant of spectrum 10 corresponds to a spacing of approximately 2.2 kilometers between bands in the image. A less well-defined peak corresponding to wavelengths of 1.3 kilometers can be seen in spectrum 1. This peak appears to be broader

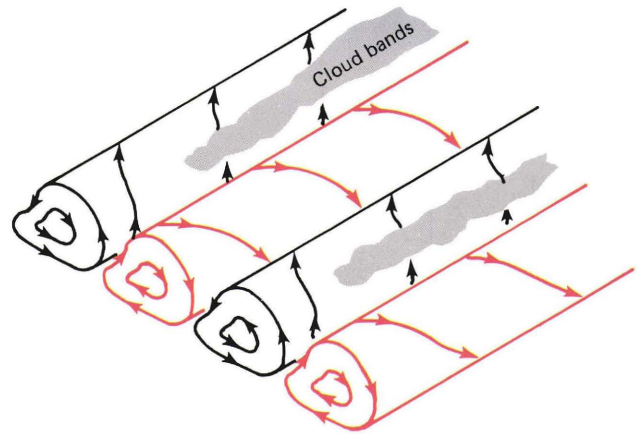


**Figure 7**—Typical roll vortices in the planetary boundary layer. The roll axis is aligned with the direction of local wind.

in angular extent, as might be expected since the corresponding image structure is not as strongly banded and uniform as that of image 10. However, the directionality is still clearly evident. Nearly all of the spectra exhibit a low wave number directionality that is more clearly evident than in the corresponding imagery.

Some of the spectra of Fig. 8 appear to specify more than one direction, such as spectrum 9, which contains two radial bands of approximately equal intensity separated by about 60 degrees. Also, as discussed earlier, the spectrum of image 1 appears to be of larger angular extent than others. Computing spectra of smaller 6.4-kilometer-square images will show that this spectral complexity is really a spatial variability, regardless of whether it is real wind variability.

Figure 9 displays the 36 spectra of the 6 by 6 array of 6.4-kilometer-square images that were partitioned from MDA image 1. Peaks are clearly evident in nearly all of them, and some of the spectra even have multiple peaks. Since a spectrum will always have an even number of peaks due to radial symmetry, multiple as used here implies four or more peaks. If the peaks are interpreted as windrow signatures, then the resulting wavelengths indicate cross-row spacing, and the direction from the spectral origin to the peak will be orthogonal to the roll axis (which approximates wind direction). It should be mentioned that the processing performed (detrrending and tapering) may modify the spectral wind-direction signature by removing energy near the spectral origin but will not change the direction estimate.

## THE PASS 1339 WIND FIELD

The most interesting portion of the pass 1339 wind field is the region south of about 36 degrees north that is observed with the first twelve 40-kilometer-square SAR images. North of 36 degrees, the wind speed falls below 3 meters per second; currents, eddies, and bathymetry also influence the SAR images. Each of the original 40-kilometer-square MDA images was partitioned into a 6 by 6 array of 6.4-kilometer-square im-

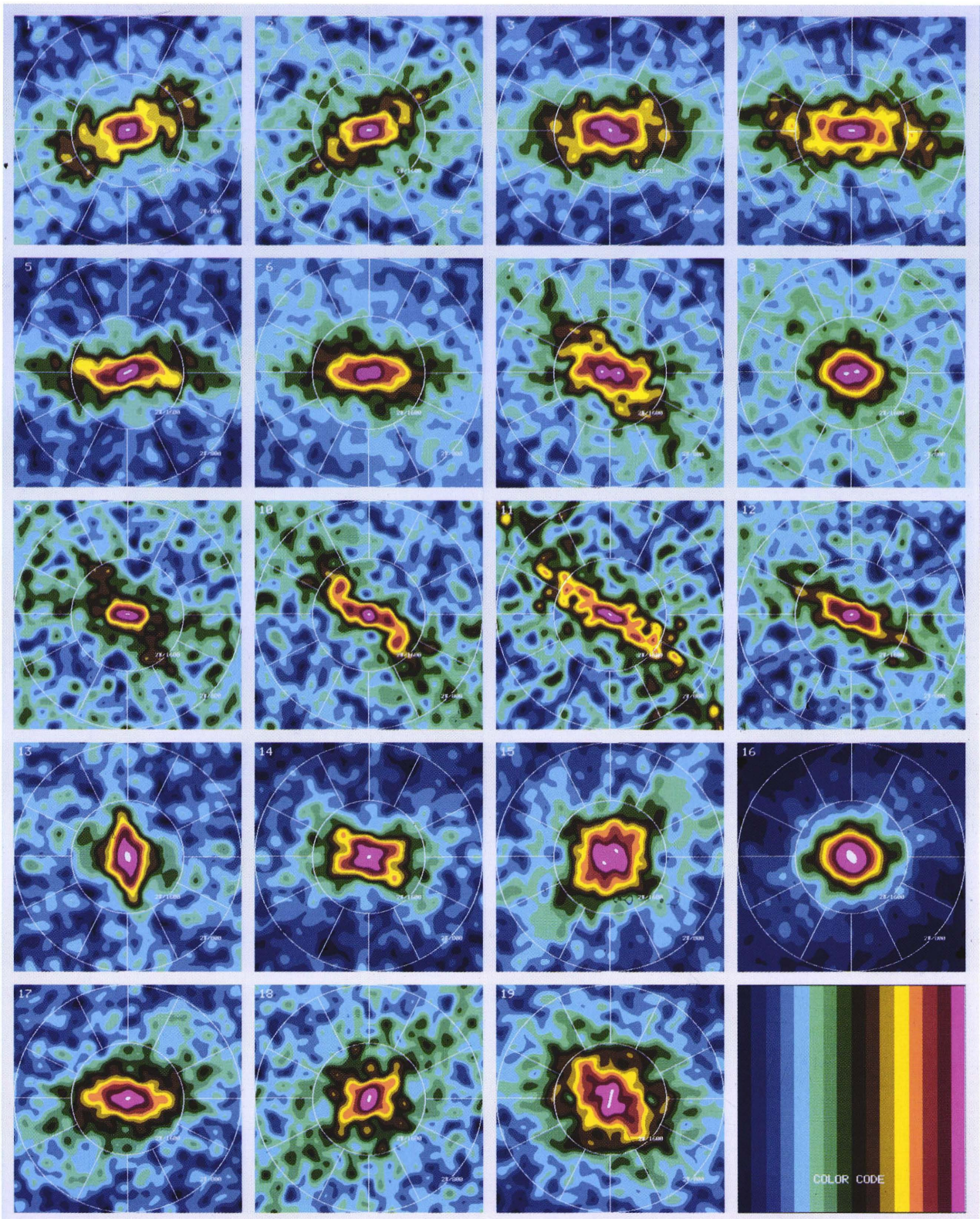


**Figure 8**—Log spectra of eighteen 25.6-kilometer-square SAR images of Fig. 2. Wavelengths displayed are from 25.6 to 0.8 kilometers. Generally, the short axis of the central elongated structure indicates wind direction. Peaks that may correspond to windrows are evident in several of the spectra.

ages, for a total of 432 images and associated spectra in this data set. To summarize the results, by noting peak locations in smoothed spectra of tapered,

detrended 6.4-kilometer-square SAR images, direction estimates were produced for approximately 95 percent of the 432 images analyzed. In 62 percent of these, only

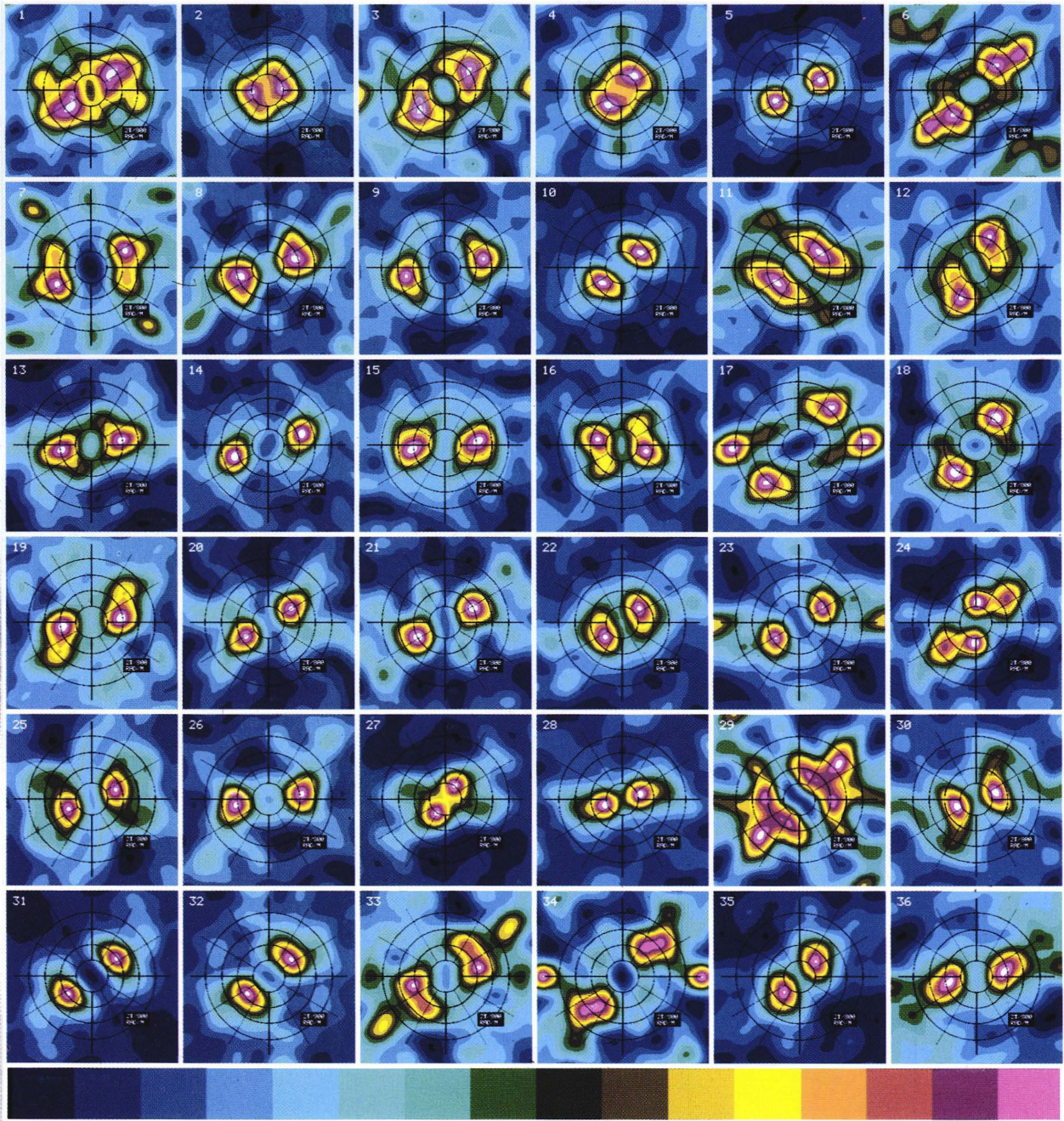
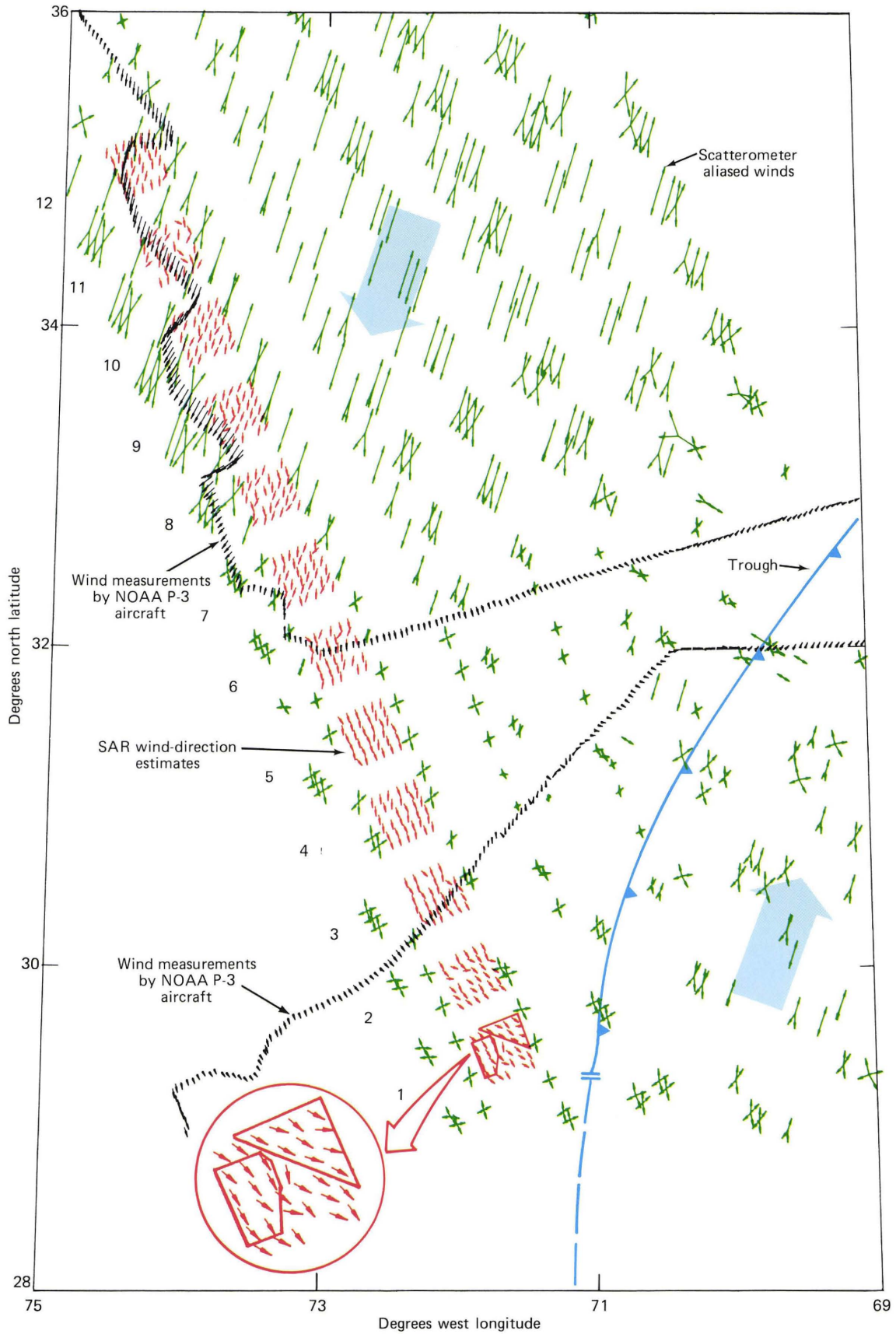


Figure 9—The 6 by 6 array of spectra of 6.5-kilometer-square subimages of image 1.

one peak was present, resulting in a 180-degree ambiguity in estimated direction. In the spectra with multiple peaks, the direction can be selected by first making the two-solution cases unambiguous and then using the information for the other cases. The error in direction determined from peak location is typically 12 degrees, which is often significantly smaller than the observed variabilities of 6 by 6 groupings of SAR direction estimates relative to their group average. Estimates derived from images 2, 8, 9, and 11 appear to be of lower quality than the others by a number of measures.

Figure 10 is a map of all the wind-direction estimates produced by SASS, SAR, and the aircraft. All the arrows indicate the direction of wind flow, and aircraft and SASS arrows are scaled to represent wind speed. The position of the trough is located as it was on the National Weather Service surface chart for 1200 Greenwich Mean Time, which was about 3 hours prior to overpass. There is always a 180-degree ambiguity in the SAR direction estimates because of the radial symmetry of the spectra. This ambiguity was removed by considering the overall circulation, along with unambiguous aircraft measurements. SASS is unambig-



**Figure 10**—Map of wind-field estimates from SASS, aircraft, and SAR at 6.4-kilometer resolution for pass 1339. The region shown is indicated in Fig. 1.



uous in two regions, which are marked by large arrows in Fig. 10. At these locations, the wind direction is about 45 degrees relative to the transit direction of the spacecraft. In this situation, SASS will typically provide only two ambiguous wind directions, separated by 180 degrees. The correct solution for these cases will be obvious since the wind circulates counterclockwise around the trough. However, mixed with these doubly ambiguous solutions are solutions with three or four possibilities. Two of the possible solutions are separated by 10 to 40 degrees, and the other one or two occur nearly 180 degrees from these. Solutions alternate among the doubly, triply, and quadruply ambiguous solutions in regions where the wind field appears to be quite uniform. The available supporting surface truth is not sufficient to determine if this is real wind field variability.

The lower three sets of SAR spectra, labeled 1, 2, and 3 in Fig. 10, reveal an interesting aspect of the wind field that would be ambiguous with SASS data alone. The direction estimates in SAR image 3 indicate a north-northwesterly flow almost exactly along track. The SAR image 2 estimates indicate a transition of the wind field depicted in image 3 to that displayed in image 1. The direction estimates from SAR image 1 show a shift of direction in the wind field, with the western estimates exhibiting the same north-northwesterly flow and consistent with a SASS alias, while those in the eastern part of the image indicate a more northwesterly flow that would form a continuous transition to the region of southwesterly flow just eastward of these locations on the other side of the trough (see the inset in Fig. 10).

In the same region, none of the SASS solutions is consistent with those of the SAR. The SASS provides one estimate at about 160 degrees from north near images 1 through 5, agreeing with the along-track flow indicated by SAR. However, there does not appear to be a SASS solution that agrees with the other flow in image 1. Moreover, the SASS solutions do not provide a continuous transition to the southwesterly flow, just eastward of image 1. In fact, to construct a smoothly varying wind field, one is required to select different aliases from SASS solutions that are nearly identical.

It can be shown<sup>13</sup> through least-squares methods that the measurement error in direction determined from peak locations is typically about 12 degrees, which is sometimes significantly smaller than the observed variabilities of 6 by 6 groupings of SAR direction estimates relative to their group average. Pierson<sup>14</sup> provides substantially smaller theoretical estimates of mesoscale wind-direction variability than we observe in our SAR direction estimates, but much of the observed variability is the result of measurement error. With this consideration in mind, the SAR high-resolution estimates are useful to delineate shifts of directions, or boundaries between flows, such as those in MDA image 1. SAR estimates within a uniform flow can be averaged to obtain more reliable estimates. If all estimates in a 6 by 6 grouping are averaged (assum-

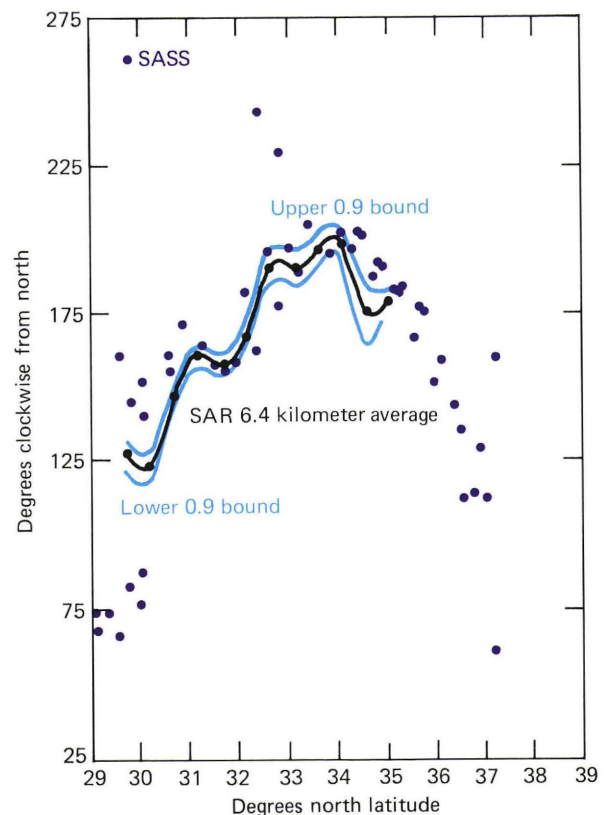
ing that averaging is appropriate), then the standard error for the mean wind direction within a 40-kilometer-square region is on the order of 2 to 3 degrees.

Figure 11 compares averages of 6.4-kilometer-square SAR image-direction estimates with scatterometer estimates plotted versus latitude. Where ambiguities with SASS remain, the two most likely solutions are plotted. Ninety percent confidence limits on the average direction determined for each MDA image are also shown. Directions determined from spectra of 25.6-kilometer-square images are shown in Ref. 13 and do not differ significantly from the SAR estimates plotted here. Agreement is good, the only discrepancy occurring in the bottom two MDA images near the base of the trough.

### SUMMARY

There is a need to measure the ocean-surface vector wind field for a variety of scientific objectives and applications. The utility of satellite microwave scatterometry was demonstrated with SASS, and another improved scatterometer will be flown on the Navy Remote Ocean Sensing System in 1989.

The Seasat SAR, at least under some conditions, is also capable of remotely sensing the vector wind field.



**Figure 11**—Measured wind direction (SASS and SAR) versus latitude for pass 1339. The 6.4-kilometer average estimate is the average of the direction estimates (approximately 30) derived from the array of 6.4-kilometer subimagery extracted from each of the first 12 MDA 40-kilometer-square SAR images. Also indicated is the 90 percent confidence limit for each of these averages.

Moreover, the high resolution possible with SAR makes it possibly the best choice for situations in which high-resolution wind field measurements are important, such as near fronts, squall lines, and environments of high wind gradient.

Although the SAR data set from pass 1339 is limited in spatial and temporal extent, the results obtained in this wind field analysis are sufficiently encouraging that other data sets representing varied environmental conditions should be analyzed. The analysis will help determine the SAR's capability for remote wind sensing over a wider range of surface conditions.

## REFERENCES

- <sup>1</sup>"Special Issue on the Seasat-1 Sensors," *IEEE J. Oceanic Eng.* **OE-5** (1980).
- <sup>2</sup>"Seasat Special Issue I: Geophysical Evaluation," reprint, *J. Geophys. Res.* **87** (1982).
- <sup>3</sup>"Seasat Special Issue II: Scientific Results," reprint, *J. Geophys. Res.* **88** (1983).
- <sup>4</sup>J. F. Vesceky and R. H. Stewart, "The Observation of Ocean Surface Phenomena Using Imagery from the Seasat Synthetic Aperture Radar: An Assessment," *J. Geophys. Res.* **87**, 3397-3430 (1982).
- <sup>5</sup>R. A. Brown, "On a Satellite Scatterometer as an Anemometer," *J. Geophys. Res.* **88**, 1663-1673 (1983).
- <sup>6</sup>R. C. Beal, T. W. Gerling, D. E. Irvine, F. M. Monaldo, and D. G. Tilley, "Spatial Variations of Ocean Wave Directional Spectra from the Seasat Synthetic Aperture Radar," *J. Geophys. Res.* (in press, 1986).
- <sup>7</sup>R. K. Moore and A. K. Fung, "Radar Determination of Winds at Sea," in *Proc. IEEE* **67**, 1504-1521 (1979).
- <sup>8</sup>T. W. Thompson, D. E. Weissman, and F. I. Gonzalez, "L-Band Radar Backscatter Dependence upon Surface Wind Stress: A Summary of New Seasat-1 and Aircraft Observations," *J. Geophys. Res.* **88**, 1727-1735 (1983).
- <sup>9</sup>M. G. Wurtele, P. M. Woiceshyn, S. Peteherych, M. Borowski, and W. S. Appleby, "Wind Direction Alias Removal Studies of Seasat Scatterometer-Derived Wind Fields," *J. Geophys. Res.* **87**, 3365-3377 (1982).
- <sup>10</sup>L. L. Fu and B. Holt, *Seasat Views Oceans and Sea Ice with Synthetic Aperture Radar*, JPL Pub. 81-120, Jet Propulsion Laboratory, Pasadena, p.108 (1982).
- <sup>11</sup>R. A. Brown, "Longitudinal Instabilities and Secondary Flows in the Planetary Boundary Layer: A Review," *Rev. Geophys. Space Phys.* **18**, 683-697 (1980).
- <sup>12</sup>A. H. Woodcock, "Soaring Over the Open Sea," *Sci. Mon.* **55**, 226-232 (1942).
- <sup>13</sup>T. W. Gerling, "Structure of the Surface Wind Field from the Seasat SAR," *J. Geophys. Res.* (in press, 1986).
- <sup>14</sup>W. J. Pierson, "The Measurements of the Synoptic Scale Wind over the Ocean," *J. Geophys. Res.* **88**, 1683-1708 (1983).

## THE AUTHOR

THOMAS W. GERLING was born in LaCrosse, Wis., in 1954. He received a B.S. degree in mathematics and in physics from the Massachusetts Institute of Technology in 1976 and an M.S. degree in statistics from the University of Chicago in 1978. Before joining APL's Space Geophysics Group in 1981, Mr. Gerling had worked at Woods Hole Oceanographic Institution, the U.S. Department of Energy, and in the Strategic Systems Department at APL. His present work at APL is concerned with the analysis of spaceborne measurements of ocean winds and waves.

